Geochemistry, Geophysics, Geosystems

RESEARCH ARTICLE
10.1029/2019GC008663

Plume-Induced Subduction Initiation: Single-Slab or Multi-Slab Subduction?

Marzieh Baes[1], Stephan Sobolev[1,2], Taras Gerya[3], and Sascha Brune[1,2]

[1]GFZ German Research Center for Geosciences, Potsdam, Germany, [2]Institute of Geosciences, University of Potsdam, Potsdam, Germany, [3]Department of Earth Sciences, ETH-Zurich, Zurich, Switzerland

Key Points:
- In present-day Earth plume-lithosphere interaction leads to single-slab, multi-slab, or no subduction initiation
- In Archean times plume-lithosphere interaction could result in either multi-slab subduction or episodic short-lived circular subduction
- Extension facilitates plume-induced subduction initiation

Supporting Information:
- Supporting Information S1

Correspondence to:
M. Baes,
baes@gfz-potsdam.de

Citation:
Baes, M., Sobolev, S., Gerya, T., & Brune, S. (2020). Plume-induced subduction initiation: Single-slab or multi-slab subduction?. *Geochemistry, Geophysics, Geosystems*, *21*, e2019GC008663. https://doi.org/10.1029/2019GC008663

Received 28 AUG 2019
Accepted 6 DEC 2019
Accepted article online 30 JAN 2020

Abstract Initiation of subduction following the impingement of a hot buoyant mantle plume is one of the few scenarios that allow breaking the lithosphere and recycling a stagnant lid without requiring any preexisting weak zones. Here, we investigate factors controlling the number and shape of retreating subducting slabs formed by plume-lithosphere interaction. Using 3-D thermomechanical models we show that the deformation regime, which defines formation of single-slab or multi-slab subduction, depends on several parameters such as age of oceanic lithosphere, thickness of the crust and large-scale lithospheric extension rate. Our model results indicate that on present-day Earth multi-slab plume-induced subduction is initiated only if the oceanic lithosphere is relatively young (<30–40 Myr, but >10 Myr), and the crust has a typical thickness of 8 km. In turn, development of single-slab subduction is facilitated by older lithosphere and pre-imposed extensional stresses. In early Earth, plume-lithosphere interaction could have led to formation of either episodic short-lived circular subduction when the oceanic lithosphere was young or to multi-slab subduction when the lithosphere was old.

1. Introduction

The formation of new subduction zones is a key component of global plate tectonics (Bercovici, 2003; Gurnis et al., 2004; Stern & Gerya, 2018). It is commonly accepted that the negative buoyancy of cold and dense oceanic lithosphere provides the major driving force of subduction once it becomes self-consistent. However, in order to initiate subduction, the lithosphere has to be broken, which is most likely to occur in places of reduced strength that feature, for instance, a pre-existing weakness zone in the lithosphere (McKenzie, 1977; Mueller & Phillips, 1991; Stern, 2004; Stern & Gerya, 2018). This kind of pre-existing weakness might be created in a variety of tectonic settings such as transform/fracture zones, extinct mid-ocean ridges or back-arc regions of mature subduction zones. Subduction initiation along a transform/fracture zone or a mid-ocean ridge follows from a change in the relative plate motion (Hall et al., 2003; Lebrun et al., 2003; Pearce et al., 1992; Uyeda & Ben-Avraham, 1972). Subduction initiation in backarc of mature subduction zones occurs as a result of entering of buoyant continental crust or oceanic plateau to the subduction system (Cowley et al., 2004; Hathway, 1993; Kroenke, 1989; Phinney et al., 2004; Stern, 2004; Wells, 1989; Yan & Kroenke, 1993).

Despite the lack of any Cenozoic examples, other widely accepted locations of subduction initiation are passive margins (Cloetingh et al., 1982, 1984, 1989; Faccenna et al., 1999; Nikolaeva et al., 2010; Regenauer-Lieb et al., 2001; Stern, 2004; Stern & Gerya, 2018). The broad acceptance of these tectonic settings arises from the role that they play in closing phase of the Wilson cycle (Wilson, 1966). Since both passive margins and pre-existing weakness zones in the lithosphere are products of plate tectonics this concept cannot address the question of "how did the first subduction zone form on Earth?"

A recently proposed scenario that is independent of plate tectonics and can thus start recycling of a stagnant planetary lid is plume-induced subduction initiation (Baes et al., 2016; Gerya et al., 2015; Stern & Gerya, 2018; Ueda et al., 2008). According to this scenario, upon arrival of a hot and buoyant mantle plume beneath the lithosphere, the lithosphere breaks apart and the hot mantle plume materials flow atop of the broken parts of the lithosphere. This leads to bending of the lithosphere and eventually initiation of subduction. Plume-lithosphere interaction can lead to subduction initiation provided that the plume causes a critical local weakening of the lithospheric material above it, which depends on the plume volume, its buoyancy, and the thickness of the lithosphere (Ueda et al., 2008). Burov and Cloetingh (2010) noted that initiation of continental lithosphere subduction is plausible following interaction of a plume with a continental

lithosphere. They indicated that key factors in subduction of continental lithosphere to depths of 300–500 km are the rheological stratification of lithosphere and its free surface. Gerya et al. (2015) showed that three factors play key roles in subduction initiation that are (a) strong, negatively buoyant oceanic lithosphere; (b) magmatic weakening above the plume; and (c) lubrication of the slab interface by hydrated crust. They indicated that in the early Earth plume-lithosphere interaction could result in subduction initiation only if the oceanic plate was older than 10 Myr. According to that study, episodic lithospheric drips were the result of interaction between a plume with a younger plate in the early Earth. Plume-lithosphere interaction in present-day Earth could lead to four different deformation regimes: (a) self-sustaining subduction initiation; (b) frozen subduction initiation; (c) slab break-off; and (d) plume underplating (Baes et al., 2016). These responses depend on several parameters, such as the size, composition and temperature of the plume, the brittle/plastic strength and age of the oceanic lithosphere, and the presence/absence of lithospheric heterogeneity (Baes et al., 2016).

Geochemical, geochronological, and isotope data have recently provided strong evidence for plume-induced subduction initiation in the Central American region (Whattam & Stern, 2014). At about 100–95 Ma the arrival of a large plume head, which formed the Caribbean Large Igneous Province, induced a new subduction zone in this region. Compositional and density contrasts between the 140–110 Myr oceanic plateau and a normal old oceanic lithosphere created favorable conditions for subduction initiation upon arrival of a mantle plume beneath the lithosphere (Whattam & Stern, 2014). Boschman et al. (2019), using plate kinematic reconstructions indicated that the subduction in western Caribbean was formed in an intra-oceanic environment as a result of plume-lithosphere interaction at about 100 Ma. The formation of the Cascadia subduction zone in Eocene times was recently suggested as a second example of plume-induced subduction initiation (Stern & Dumitru, 2019).

Previous modeling studies (Baes et al., 2016; Gerya et al., 2015; Ueda et al., 2008) showed that plume-lithosphere interaction can result in initiation of multi-slab or single-slab subduction zones around the newly formed plateau. However, they did not explore the factors playing key roles in discriminating between the single-slab and multi-slab subduction scenarios. The reconstruction model of Whattam and Stern (2014) suggests that the arrival of plume head beneath the lithosphere at 100 Ma led to the formation of a single-slab subduction zone along the west and southwest Caribbean plate, which raises the question of why was subduction initiated only on one side of Caribbean plateau? Whattam and Stern (2014) argued that the main reason for initiation of single-slab subduction zone in Caribbean region was the existence of the Puerto Rico/Lesser Antilles subduction zones around the northeastern Caribbean that were formed tens of million years before subduction initiation in the west and southwest of the region. On the other hand, according to the reconstruction of Whattam and Stern (2014), at the time of arrival of mantle plume near the surface, there was an older oceanic plateau (with an age of nearly 40 Myr at the time of plume-lithosphere interaction) in the back-arc region of the Puerto Rico/Lesser Antilles trenches. From the curved shape of trenches at 100 Ma it is inferred that the slab was probably rolling back, having led to an extensional regime in the back-arc area. It is important therefore to investigate the effect of additional factors, which might affect formation of single-slab subduction zone in the Caribbean region such as the existence of the old oceanic plateau above the plume head and the extensional regime in the back-arc area of Puerto Rico/Lesser Antilles subduction zones.

Based on the above considerations, the present study aims to address two key unexplored questions for plume-induced subduction initiation: Which lithospheric parameters play key roles in defining either single-slab or multi-slab subduction initiation? And what is the impact of regional extension on plume-lithosphere interaction? Here, we will answer these questions by using 3-D numerical models and by linking the results to the formation of single-slab subduction in the northwest of South America and west of the Caribbean plate.

2. Numerical Model Description

We use the code I3ELVIS, which solves the momentum, continuity, and energy equations based on a staggered finite difference scheme combined with a marker-in-cell technique (Gerya, 2010):

$$\frac{D\rho}{Dt}+\rho\nabla.\vec{v}=0,\frac{\partial\sigma_{ij}}{\partial x_j}-\frac{\partial P}{\partial x_i}+\rho g_i=0,\rho C_P\left(\frac{DT}{Dt}\right)=-\nabla.\vec{q}+H_r+H_a+H_s+H_l \quad (1)$$

where $\frac{D}{Dt}$, P, ρ, v, σ_{ij}, and g_i are Lagrangian time derivative, pressure, density, velocity, Cauchy stress and gravity acceleration, respectively. C_P and q denote heat capacity and heat flux while H_r,H_a,H_s, and H_l stand for radioactive, adiabatic, shear, and latent heating, respectively.

Our model domain covers a volume of 1212 × 296 ×1212 km, which is resolved by 404 × 148 × 404 grid points with a resolution of 3 × 3 km in the horizontal (x-z) plane and 2 km in the vertical (y) direction. More than 235 million markers are employed for advecting various material properties and temperatures. The model consists of a 20 km thick layer of sticky air simulating an internal free surface, an oceanic lithosphere, a spherical plume with radius of 100 km, and asthenosphere until depth of 296 km (Figure 1). The oceanic lithosphere is composed of upper and lower crust. The upper crust has a thickness of 2 km and thickness of lower crust varies from 6 km (typical 8 km thickness of oceanic crust) to 28 km (representing a 30 km oceanic plateau) in different models (Table 2). The thickness of the oceanic lithosphere, which is defined thermally, varies from 50 to 92 km corresponding to lithospheric age of 20 to 70 Myr in different experiments. We use non-Newtonian viscoplastic rheologies (Ranalli, 1995) for different layers of our model (Table 1). The upper crust, lower crust, plume, and mantle are considered to be wet quartzite, plagioclase An75, wet olivine, and dry olivine, respectively.

The viscosity in our models depends on stress, temperature and pressure. The effective viscosity is expressed as

$$\frac{1}{\eta_{effectiv}} = \frac{1}{\eta_{diffusion}} + \frac{1}{\eta_{dislocation}} \tag{2}$$

where $\eta_{diffusion}$ and $\eta_{dislocation}$ are viscosities for diffusion and dislocation creep, respectively, and are defined as

$$\eta_{diffusion} = {}^{1}\!/_{2}\frac{A_D}{\sigma_{cr}^{n-1}}\exp\left(\frac{E+PV}{RT}\right) \quad \eta_{dislocation} = {}^{1}\!/_{2}A_D{}^{1}\!\Big/_{n}exp\left(\frac{E+PV}{RT}\right)\dot{\varepsilon}_{II}^{(1-n)/n} \tag{3}$$

in which P is the pressure, T is temperature, $\dot{\varepsilon}_{II} = \sqrt{\frac{1}{2}\dot{\varepsilon}_{ij}\dot{\varepsilon}_{ij}}$ is the second invariant of the strain rate tensor, σ_{cr} is the diffusion-dislocation creep transition stress, and A_D, E, V, and n are strain rate pre-exponential factor, activation energy, activation volume, and stress exponent, respectively. We limit the viscosity to the range between 1×10^{18} and 1×10^{26} Pa s.

We use the following modified version of Drucker-Prager yield criterion (Byerlee, 1978; Ranalli, 1995) to define plastic deformation:

$$\tau = C + \phi\lambda_{melt}P \tag{4}$$

where C is the rock strength at $P = 0$, λ_{melt} is the melt-induced weakening factor (Gerya et al., 2015), and ϕ is the internal friction coefficient for the confined fractures. The product of $\phi\lambda_{melt}$ is called effective friction coefficient. We note that melt-induced weakening is implemented locally within the lithosphere above areas of melt extraction. For all other materials, no magmatic weakening is assumed ($\lambda_{melt} = 1$).

All the model boundaries are free slip boundaries, except at the bottom of the model, which is an open permeable boundary. In some models we impose some kinematic boundary conditions on the right and left sides of the model simulating an extensional regime (Model M36–M59 in Table 2). In these models the imposed outflow is compensated by the inflow at the bottom boundary to conserve mass globally in the model.

The initial temperature of the oceanic lithosphere is calculated based on cooling half space formulation (Turcotte & Schubert, 1982). We consider oceanic lithospheres with different ages to investigate the effect of oceanic lithospheric age on the plume-lithosphere interaction (Table 2). The temperature in the asthenosphere is adiabatic with a gradient of ~0.5 K km^{-1}. The temperature of the plume is constant, varying between 1850 and 2050 K in different experiments. The thermal boundary conditions are 273 K at the upper boundary and zero horizontal heat flux across the vertical boundaries. An infinity-like external temperature condition (Gerya, 2010) is imposed on the lower boundary. In some models, we consider a 200 K higher temperature at the lower boundary to simulate a plume with a tail (M60–M107 in Table 2).

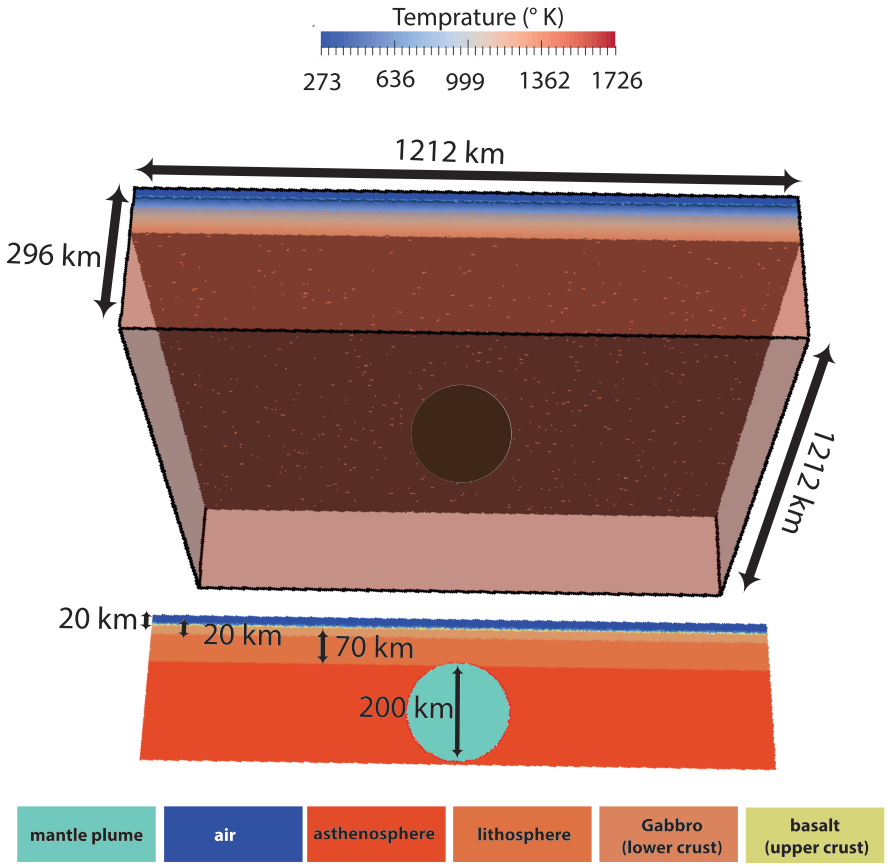

Figure 1. Initial model setup (model M4 in Table 2). The upper panel shows the initial temperature field of the model. The lower panel, illustrating a cross-section cutting through the middle of model, represents the compositional field (color code is at the bottom of the figure).

Density in our experiments depends on pressure and temperature:

$$\rho = \rho_0[1-\alpha(T-T_0)][1+\beta(P-P_0)] \tag{5}$$

where ρ_0 and T_0 are the density under the conditions of $P_0 = 0.1$ MPa and $T_0 = 298$ K (pressure and temperature at Earth's surface) and α and β are the thermal expansion coefficient and the compressibility coefficient, respectively.

Melt extraction and melt percolation are defined in a simplified manner as described in (Gerya, 2013; Gerya et al., 2015). Melt extraction is tracked by Lagrangian markers. The total amount of melt, M, for every marker is calculated as

$$M = M_0 - \Sigma_m M_{\text{ext}} \tag{6}$$

where M_0 is the standard volumetric degree of mantle melting and $\Sigma_m M_{\text{ext}}$ is the total melt fraction extracted during the previous melt extraction episodes. The extracted melt moves vertically and is added to the top of the shallowest partially molten mantle above the plume and forms volcanic rocks. Melt percolation is not modeled directly and is considered to be instantaneous (Connolly et al., 2009).

Crystallization of magma and melting of the crust are computed from the simple linear batch melting model (Gerya, 2013)

$$\begin{aligned} &M = 0 \text{ when } T<T_{solidus}, \\ &M = (T-T_{solidus})/(T_{liquidus}-T_{solidus}) \text{ when } T_{solidus}<T<T_{liquidus}, \\ &M = 1 \text{ when } T>T_{liquidus} \end{aligned} \tag{7}$$

Table 1
Rheological Parameters of Different Layers of the Model

Material	Flow law[a]	ρ (kg m^{-3})	C (MPa)	φ (-)	A (Pa^n s)	E (kJ mol^{-1})	V (m^3 mol^{-1})	n	K (W m^{-1} K^{-1})	H (μW m^{-3})
Upper crust	Wet quartz	3,000	1	0.1	1.97×10^{17}	154	0	2.3	$1.18 + 474/(T + 77)$	0.25
Lower crust	Plagioclas An75	3,000	1	0.2	4.8×10^{22}	238	0	3.2	$1.18 + 474/(T + 77)$	0.25
Lithospheric mantle	Dry olivine	3,300	1	0.2	3.9×10^{16}	532	0.8×10^{-5}	3.5	$0.73 + 1293/(T + 77)$	0.022
Asthenosphere	Dry olivine	3,300	1	0.2	3.9×10^{16}	532	0.8×10^{-5}	3.5	$0.73 + 1293/(T + 77)$	0.022
Plume	Wet olivine	3,000	1	0.2	5.01×10^{20}	470	0.8×10^{-5}	4	$0.73 + 1293/(T + 77)$	0.022

Note. See text for further explanation.
[a]Flow law for all materials are based on Ranalli (1995).

where $T_{\text{solidus}} = 1327 + 0.091P$ and $T_{\text{liquidus}} = 1423 + 0.105P$ are solidus and liquidus temperature of the crust at a given pressure P, respectively. The effective density of the mafic magma and molten crust is defined as (Gerya, 2013)

$$\rho_{eff} = \rho_{solid}(1-M+M)\frac{\rho_{0molten}}{\rho_{0solid}} \tag{8}$$

where $\rho_{\text{solid}} = 3{,}000$ kg/m^3 and $\rho_{0\text{molten}} = 2{,}800$ kg/m^3 are the standard densities of solid and molten crust, respectively and ρ_{solid} is the density of solid crust at given P and T, which is calculated as

$$\rho_{\text{solid}} = \rho_{0\text{solid}}\times(1-\alpha(T-298))\times(1+\beta(P-0.1)) \tag{9}$$

where $\alpha = 3 \times 10^{-5}$ 1/K and $\beta = 10^{-5}$ 1/MPa are thermal expansion and compressibility of the crust, respectively.

Slab dehydration and mantle hydration are based on the water markers approach (Gerya & Meilick, 2011) in which the equilibrium mineralogical water content for the crust and the mantle is defined as a function of pressure and temperature from thermodynamic data by free energy minimization. Fluid markers simulate upward motion of released water by slab dehydration process. The fluid markers migrate upwards and release water when they reach a rock with capability of assimilating water by hydration or melting reactions at given PT-conditions and rock composition. Eclogitization of subducted crust is modeled as a linearly increase of density with pressure from 0% to 16% in the PT region between the experimentally determined garnet-in and plagioclase-out phase transitions in basalt (Ito & Kennedy, 1971).

3. Model Results

In our model suite we investigate the effect of thickness of the crust, mantle temperature, extension rate, and plume tail on the response of the lithosphere to plume-lithosphere interaction. Since one of the controlling factor in the lithospheric deformation is the age of lithosphere, we vary lithospheric age along with aforementioned parameters to study the effect of each of them on plume-lithosphere interaction. Altogether we conducted 107 experiments, which are listed in Table 2.

We found four distinctly different lithospheric deformation patterns: (a) multi-slab subduction initiation, (b) single-slab subduction initiation, (c) plateau formation without subduction initiation, and (d) episodic short-lived circular subduction initiation. Below we show the results for some of our models, which represent different deformation patterns in response to changes in specific model parameters.

3.1. Effect of Crustal Thickness

Models with different thickness of the crust and oceanic lithospheric ages show diverse responses to plume-lithosphere interaction. Based on our numerical model results three deformation patterns are achieved that are (a) multi-slab subduction initiation, (b) single-slab subduction initiation, and (c) plateau formation without subduction initiation.

(a) Multi-slab subduction initiation

Table 2
List of Experiments

	Temp. of mantle (°K)	Temp. of plume (°K)	Age:thickness of oceanic plate (Myr:km)	Thickness of crust (km)	Extra conditions	State of deformation
M1	1573	1858	20:50	20	—	No subduction
M2	1573	1858	30: 60	20	—	No subduction
M3	1573	1858	40:70	20	—	No subduction
M4	1573	1858	50:77	20	—	No subduction
M5	1573	1858	60:85	20	—	No subduction
M6	1573	1858	70:92	20	—	No subduction
M7	1573	1858	20:50	16	—	No subduction
M8	1573	1858	30:60	16	—	No subduction
M9	1573	1858	40:70	16	—	No subduction
M10	1573	1858	50:77	16	—	No subduction
M11	1573	1858	60:85	16	—	No subduction
M12	1573	1858	70:92	16	—	No subduction
M13	1573	1858	20:50	12	—	No subduction
M14	1573	1858	30:60	12	—	No subduction
M15	1573	1858	40:70	12	—	single-slab subduction
M16	1573	1858	50:77	12	—	No subduction
M17	1573	1858	60:85	12	—	No subduction
M18	1573	1858	70:92	12	—	No subduction
M19	1573	1858	20:50	8	—	Multi-slab subduction
M20	1573	1858	30:60	8	—	Single-slab subduction
M21	1573	1858	40:70	8	—	Single-slab subduction
M22	1573	1858	50:77	8	—	No subduction
M23	1573	1858	60:85	8	—	No subduction
M24	1573	1858	70:92	8	—	No subduction
M25	1773	2058	20:50	20	Higher heat production in crust and mantle	Episodic short-lived circular subduction
M26	1773	2058	30:60	20	Higher heat production in crust and mantle	Episodic short-lived circular subduction
M27	1773	2058	40:70	20	Higher heat production in crust and mantle	Episodic short-lived circular subduction
M28	1773	2058	50:77	20	Higher heat production in crust and mantle	Multi-slab subduction
M29	1773	2058	60:85	20	Higher heat production in crust and mantle	Multi-slab subduction
M30	1773	2058	70:92	20	Higher heat production in crust and mantle	Multi-slab subduction
M31	1773	2058	30:60	30	Higher heat production in crust and mantle	Episodic short-lived circular subduction
M32	1773	2058	40:70	30	Higher heat production in crust and mantle	Episodic short-lived circular subduction
M33	1773	2058	50:77	30	Higher heat production in crust and mantle	Multi-slab subduction
M34	1773	2058	60:85	30	Higher heat production in crust and mantle	Multi-slab subduction
M35	1773	2058	70:92	30	Higher heat production in crust and mantle	Multi-slab subduction
M36	1573	1858	20:50	20	Applying 1 cm/yr	No subduction
M37	1573	1858	30:60	20	Applying 1 cm/yr	No subduction
M38	1573	1858	40:70	20	Applying 1 cm/yr	Single-slab subduction
M39	1573	1858	50:77	20	Applying 1 cm/yr	Single-slab subduction
M40	1573	1858	60:85	20	Applying 1 cm/yr	Single-slab subduction
M41	1573	1858	70:92	20	Applying 1 cm/yr	No subduction
M42	1573	1858	20:50	8	Applying 1 cm/yr	Single-slab subduction
M43	1573	1858	30:60	8	Applying 1 cm/yr	Single-slab subduction
M44	1573	1858	40:70	8	Applying 1 cm/yr	Single-slab subduction
M45	1573	1858	50:77	8	Applying 1 cm/yr	Single-slab subduction
M46	1573	1858	60:85	8	Applying 1 cm/yr	Single-slab subduction
M47	1573	1858	70:92	8	Applying 1 cm/yr	No subduction
M48	1573	1858	20:50	20	Applying 0.5 cm/yr	No subduction
M49	1573	1858	30:60	20	Applying 0.5 cm/yr	Single-slab subduction
M50	1573	1858	40:70	20	Applying 0.5 cm/yr	Single-slab subduction
M51	1573	1858	50:77	20	Applying 0.5 cm/yr	No subduction
M52	1573	1858	60:85	20	Applying 0.5 cm/yr	No subduction
M53	1573	1858	70:92	20	Applying 0.5 cm/yr	No subduction
M54	1573	1858	20:50	8	Applying 0.5 cm/yr	Single-slab subduction

Table 2
(continued)

	Temp. of mantle (°K)	Temp. of plume (°K)	Age:thickness of oceanic plate (Myr:km)	Thickness of crust (km)	Extra conditions	State of deformation
M55	1573	1858	30:60	8	Applying 0.5 cm/yr	Single-slab subduction
M56	1573	1858	40:70	8	Applying 0.5 cm/yr	Single-slab subduction
M57	1573	1858	50:77	8	Applying 0.5 cm/yr	Single-slab subduction
M58	1573	1858	60:85	8	Applying 0.5 cm/yr	Single-slab subduction
M59	1573	1858	70:92	8	Applying 0.5 cm/yr	No subduction
M60	1573	1858	20:50	20	Upwelling of hot mantle below the mantle plume	No subduction
M61	1573	1858	30:60	20	Upwelling of hot mantle below the mantle plume	No subduction
M62	1573	1858	40:70	20	Upwelling of hot mantle below the mantle plume	Single-slab subduction
M63	1573	1858	50:77	20	Upwelling of hot mantle below the mantle plume	No subduction
M64	1573	1858	60:85	20	Upwelling of hot mantle below the mantle plume	No subduction
M65	1573	1858	70:92	20	Upwelling of hot mantle below the mantle plume	No subduction
M66	1573	1858	20:50	16	Upwelling of hot mantle below the mantle plume	No subduction
M67	1573	1858	30:60	16	Upwelling of hot mantle below the mantle plume	No subduction
M68	1573	1858	40:70	16	Upwelling of hot mantle below the mantle plume	Single-slab subduction
M69	1573	1858	50:77	16	Upwelling of hot mantle below the mantle plume	No subduction
M70	1573	1858	60:85	16	Upwelling of hot mantle below the mantle plume	No subduction
M71	1573	1858	70:92	16	Upwelling of hot mantle below the mantle plume	No subduction
M72	1573	1858	20:50	12	Upwelling of hot mantle below the mantle plume	No subduction
M73	1573	1858	30:60	12	Upwelling of hot mantle below the mantle plume	Single-slab subduction
M74	1573	1858	40:70	12	Upwelling of hot mantle below the mantle plume	Single-slab subduction
M75	1573	1858	50:77	12	Upwelling of hot mantle below the mantle plume	No subduction
M76	1573	1858	60:85	12	Upwelling of hot mantle below the mantle plume	No subduction
M77	1573	1858	70:92	12	Upwelling of hot mantle below the mantle plume	No subduction
M78	1573	1858	20:50	8	Upwelling of hot mantle below the mantle plume	Multi-slab subduction
M79	1573	1858	30:60	8	Upwelling of hot mantle below the mantle plume	Multi-slab subduction
M80	1573	1858	40:70	8	Upwelling of hot mantle below the mantle plume	Single-slab subduction
M81	1573	1858	50:77	8	Upwelling of hot mantle below the mantle plume	Single-slab subduction
M82	1573	1858	60:85	8	Upwelling of hot mantle below the mantle plume	No subduction
M83	1573	1858	70:92	8	Upwelling of hot mantle below the mantle plume	No subduction
M84	1573	1858	20:50	20	Upwelling of hot mantle below the mantle plume + applying 1 cm/yr	Single-slab subduction
M85	1573	1858	30:60	20	Upwelling of hot mantle below the mantle plume + applying 1 cm/yr	Single-slab subduction
M86	1573	1858	40:70	20	Upwelling of hot mantle below the mantle plume + applying 1 cm/yr	Single-slab subduction
M87	1573	1858	50:77	20	Upwelling of hot mantle below the mantle plume + applying 1 cm/yr	Singe-slab subduction
M88	1573	1858	60:85	20	Upwelling of hot mantle below the mantle plume + applying 1 cm/yr	Multi-slab subduction
M89	1573	1858	70:92	20	Upwelling of hot mantle below the mantle plume + applying 1 cm/yr	No subduction
M90	1573	1858	20:50	8	Upwelling of hot mantle below the mantle plume + applying 1 cm/yr	Single-slab subduction
M91	1573	1858	30:60	8	Upwelling of hot mantle below the mantle plume + applying 1 cm/yr	Single-slab subduction
M92	1573	1858	40:70	8	Upwelling of hot mantle below the mantle plume + applying 1 cm/yr	Single-slab subduction
M93	1573	1858	50:77	8	Upwelling of hot mantle below the mantle plume + applying 1 cm/yr	Single-slab subduction
M94	1573	1858	60:85	8	Upwelling of hot mantle below the mantle plume + applying 1 cm/yr	Single-slab subduction
M95	1573	1858	70:92	8	Upwelling of hot mantle below the mantle plume + applying 1 cm/yr	Single-slab subduction
M96	1573	1858	20:50	20	Upwelling of hot mantle below the mantle plume + applying 0.5 cm/yr	No subduction
M97	1573	1858	30:60	20	Upwelling of hot mantle below the mantle plume + applying 0.5 cm/yr	No subduction
M98	1573	1858	40:70	20		Single-slab subduction

Table 2
(continued)

	Temp. of mantle (°K)	Temp. of plume (°K)	Age:thickness of oceanic plate (Myr:km)	Thickness of crust (km)	Extra conditions	State of deformation
					Upwelling of hot mantle below the mantle plume + applying 0.5 cm/yr	
M99	1573	1858	50:77	20	Upwelling of hot mantle below the mantle plume + applying 0.5 cm/yr	Single-slab subduction
M100	1573	1858	60:85	20	Upwelling of hot mantle below the mantle plume + applying 0.5 cm/yr	Single-slab subduction
M101	1573	1858	70:92	20	Upwelling of hot mantle below the mantle plume + applying 0.5 cm/yr	No subduction
M102	1573	1858	20:50	8	Upwelling of hot mantle below the mantle plume + applying 0.5 cm/yr	Multi-slab subduction
M103	1573	1858	30:60	8	Upwelling of hot mantle below the mantle plume + applying 0.5 cm/yr	Single-slab subduction
M104	1573	1858	40:70	8	Upwelling of hot mantle below the mantle plume + applying 0.5 cm/yr	Single-slab subduction
M105	1573	1858	50:77	8	Upwelling of hot mantle below the mantle plume + applying 0.5 cm/yr	Single-slab subduction
M106	1573	1858	60:85	8	Upwelling of hot mantle below the mantle plume + applying 0.5 cm/yr	Single-slab subduction
M107	1573	1858	70:92	8	Upwelling of hot mantle below the mantle plume + applying 0.5 cm/yr	No subduction

As the plume reaches the bottom of the lithosphere, it weakens the lithosphere and starts to penetrate it - Figure S1 in the supporting information data illustrates how magmatic weakening acting locally above the plume head results in breaking of the lithosphere. At the same time an oceanic plateau forms above the plume head as a result of decompression melting of the plume material (lower panel of Figure 2a showing the compositional field of model M19, which has a lithosphere of 20 Myr age and 8 km oceanic crust with present-day mantle temperature). This plateau thickens with time, leading to a growing density contrast at the plateau margins (see Figure S1 in supporting information data). When the plume breaks the whole lithosphere (see upper panel of Figure 2a showing the lithospheric stress field of model M19), it spreads within the circular region, which is formed due to the breaking of the lithosphere. Plume materials spread atop of the broken segments of the lithosphere and push them downward into the mantle. This downward displacement of the oceanic lithosphere along with density contrast within the lithosphere created by formation of a new plateau can lead to development of new circular subduction zone (Figure 2b). The ring confinement resists slab downward motion. This resistive force is eventually overcome by tearing the slab. The slabs tear due to the strain weakening, which results in a decrease of internal friction with increasing strain leading to strain localization along a shear zone (see Figure S2 in the supporting information data). Tearing the slab leads to multi-slab subduction initiation around the plateau (Figure 2c). Subduction becomes self-sustained and slabs move towards the model boundaries (Figure 2d). Model results show that under the assumptions we made multi-slab subduction initiation occurs only if the crust is thin (8 km) and if oceanic lithosphere is young—with an age of 20 Myr (Table 2 and Figure 9).

(b) Single-slab subduction initiation

Figure 3 shows the compositional and lithospheric stress fields of model M15, which has a 12 km crust and 40 Myr oceanic lithosphere with present-day mantle temperature as an example of single-slab subduction initiation. The plume breaks the lithosphere and forms a plateau above the plume head (Figure 3a). The plume materials spread within the circular area, formed due to the penetration of plume into the lithosphere. They move atop of broken parts of lithosphere and start a downward motion of the lithosphere. This leads to formation of a circular subduction (Figure 3b). Unlike experiment shown in Figure 2, here

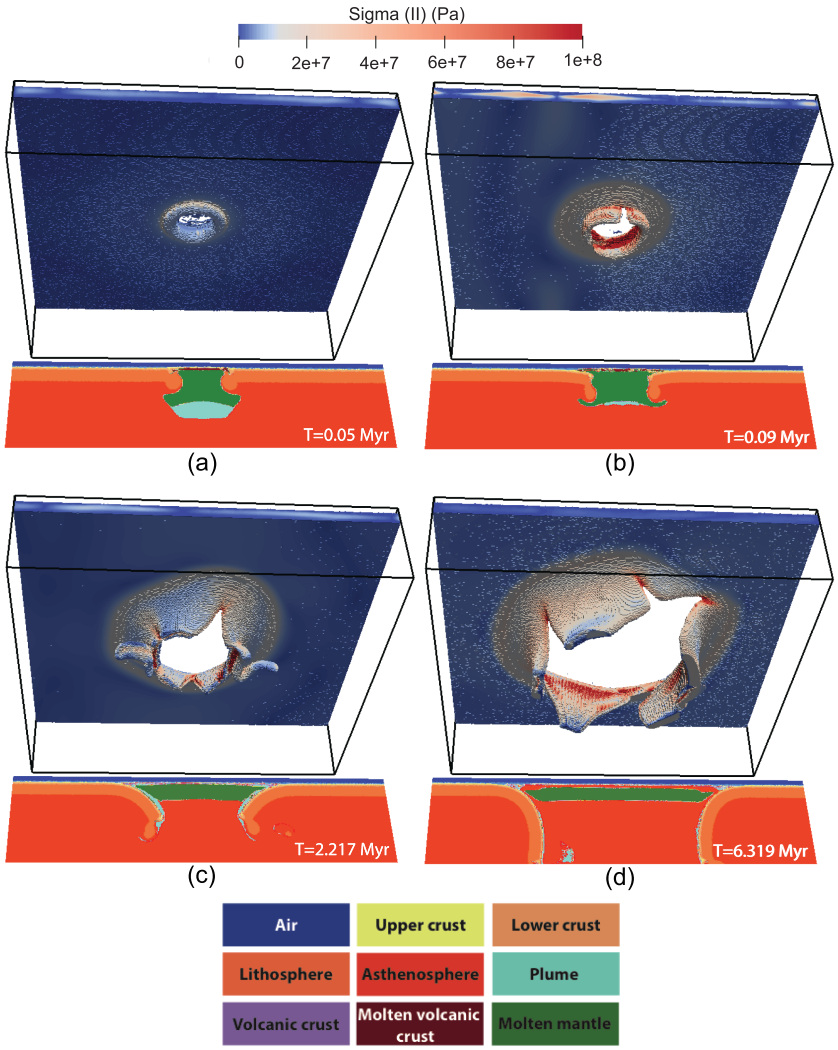

Figure 2. An example of models to investigate effect of thickness of crust (model M19 in Table 2), which illustrates formation of a multi-slab subduction zone. (a, b) The second invariant of the stress tensor within the lithosphere. (c, d) Compositional field of a 2-D cross-section cutting through center of model (color code is at the bottom of the figure).

the ring confinement is not overcome by tearing of the slab. Here, slab breaks off from one side of the circular subduction and sinks into the mantle. Extra negative buoyancy induced form detached slab facilitates subduction of slab which is still attached to the surface (Figure 3c). A single-slab subduction zone forms and retreats spontaneously towards the boundary of the model (Figure 3d). The lithospheric response to plume-lithosphere interaction is single-slab subduction initiation if the crust is thin (8 km) and the age of oceanic lithosphere is between 30 and 40 Myr or when the lithosphere has an age of 40 Myr and crustal thickness of 12 km (Table 2 and Figure 9).

(c) Plateau formation without subduction initiation

Following plume-lithosphere interaction, the plume breaks the lithosphere and forms a volcanic crust in the circular region created in the middle of the model, which indicates formation of a new oceanic plateau (Figure 4a showing the compositional and lithospheric stress fields of model M12 in Table 2). The plume materials spread atop of the broken lithosphere leading to bending of the lithosphere downward. However, due to the resistance of lithosphere to descending, subduction is not formed (Figure 4b). The deformation regime following plume-lithosphere interaction is plateau formation without subduction initiation when either the crust is thicker than 12 km or the oceanic lithosphere is older than 50 Myr (Table 2 and Figure 9).

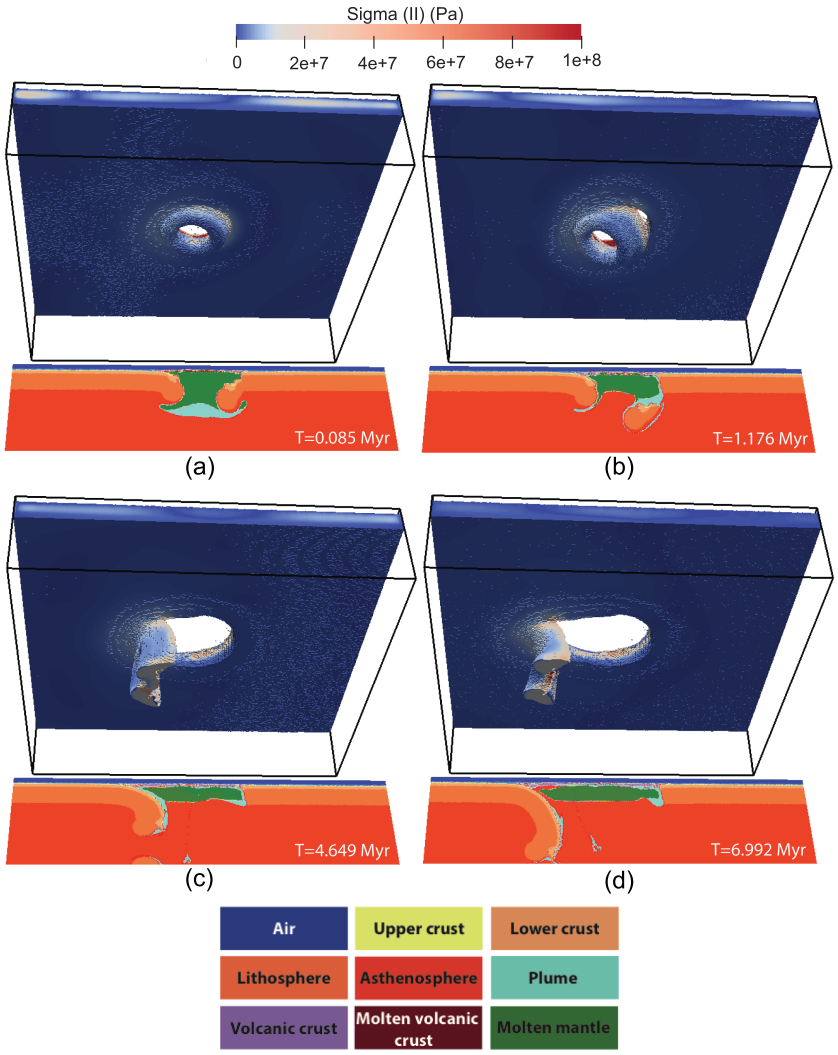

Figure 3. An example of models to investigate effect of thickness of crust (model M15 in Table 2) showing single-slab subduction initiation. For explanation of panel meanings, see Figure 2 caption.

3.2. Effect of Extension Rate

Here we impose some kinematic boundary conditions to the left and right sides of the model. We vary both age of the lithosphere and extension rate in different models. To investigate the effect of extension rate on the thickness of the crust we run experiments with two crustal thickness of 8 (typical thickness of oceanic crust) and 20 km (representing a plateau). Experiments with extension rates of 0.5 and 1 cm/yr and different age of lithosphere and thickness of the crust show two different deformation patterns. The lithospheric response to extension during plume-lithosphere interaction is either (a) single-slab subduction initiation or (b) plateau formation without subduction initiation. The evolution of deformation in these responses is very similar to those shown in Figures 3 and 4. Therefore, in this section we only show the latest stage of lithospheric response to plume-lithosphere interaction.

(a) Single-slab subduction initiation

The plume breaks the lithosphere and a circular subduction forms. Slab breaks off from the surface from one side, while on the other side the slab continues to subduct as a single-slab subduction. In this process breaking-off the slab from one side creates an extra driving force for the still-attached slab, helping the single-slab subduction to become self-sustained. This single-slab subduction retreats toward the side boundary of the model (Figure 5a representing the compositional and lithospheric stress fields of model M45 in

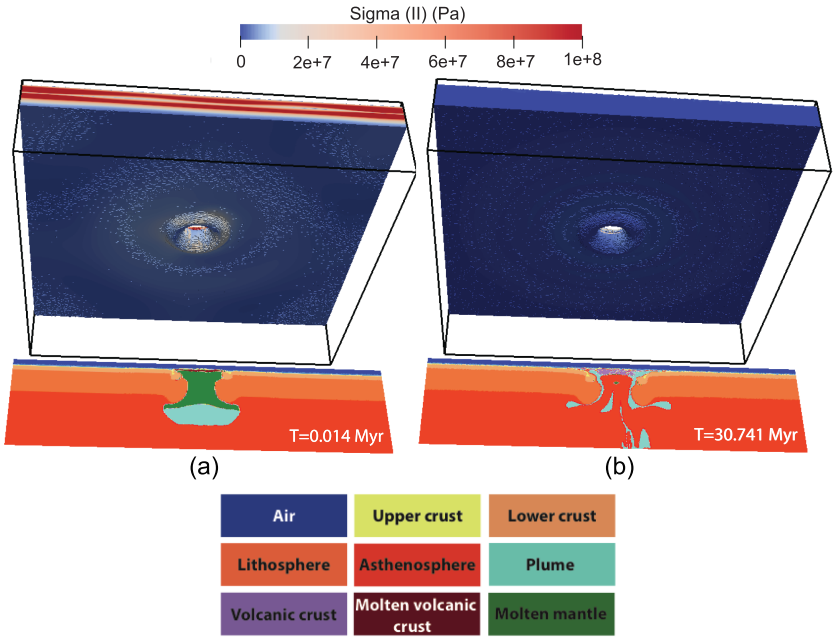

Figure 4. An example of models to investigate effect of thickness of crust (model M12 in Table 2) indicating the formation of a plateau without subduction initiation. For explanation of panel meanings, see Figure 2 caption.

Table 2). Our numerical study reveals that in a low-rate extensional regime (0.5 cm/yr) single-slab subduction of a lithosphere with a typical crustal thickness of 8 km occurs only if the age of lithosphere is less than 50 Myr. Single-slab subduction of lithospheres with thick plateau of 20 km is possible when the age of lithosphere is between 30 and 40 Myr. Higher extensional regimes facilitate subduction of older lithospheres (Table 2 and Figure 9).

(b) Plateau formation without subduction initiation

The lithosphere breaks as a result of magmatic weakening induced by arrival of a mantle plume beneath the lithosphere. A plateau forms at the surface above the plume head. Subduction is not formed due to indisposition of lithosphere to subduct. Deformation is dominated by extension and thinning of the lithosphere (Figure 5b showing the compositional and lithospheric stress fields of model M48 in Table 2). The deformation regime is plateau formation without subduction initiation when the oceanic lithosphere is old (older than 40 and 50 Myr in low- and high-rate extensional regimes, respectively; Table 2 and Figure 9). Interaction of a plume with a thick plateau of 20 km within a young lithosphere of 20 Myr also results in plateau formation without subduction initiation.

3.3. Effect of Mantle Temperature

In this section, we compare the response of the lithosphere to the arrival of a plume in Archean and present-day time. Since in Archean times, the mantle temperature, heat production in the crust as well as mantle, and crustal thickness were likely higher than those in the present-day (Herzberg et al., 2010), we run experiments with 200 K hotter mantle, higher heat production in crust and mantle (~2 times higher than those in the present day) and thicker crust (20–30 km). We vary the lithospheric age in different models. Two deformation regimes result from these experiments: (a) multi-slab subduction initiation and (b) episodic short-lived circular subduction initiation.

(a) Multi-slab subduction initiation

A plateau forms due to decomposition melting of the plume material and penetration of upwelling plume to the lithosphere (Figure 6a illustrating the compositional and lithospheric stress fields of Model M29 in Table 2). Plateau thickening is much faster than that in models with lower mantle temperature, increasing the density contrast along the margins of plateau. Plume materials spread atop of the lithosphere and push it

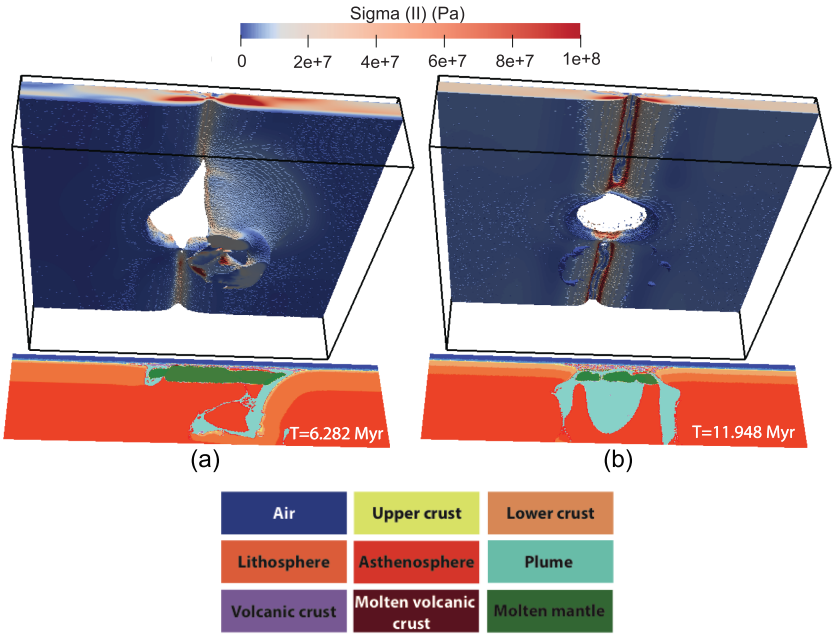

Figure 5. An example of models to investigate effect of extensional regime. Results of model: (a) M45 and (b) M48 (Table 2). For explanation of panel meanings, see Figure 2 caption.

downwards. This along with density contrast within the lithosphere results in formation of a circular slab (Figure 6b). The ring confinement, which acts as a resistive force in subduction process, is overcome by tearing of the slab and formation of multi-slab subduction (Figure 6c). Slabs subduct to greater depth with time and at the same time they retreat towards the side boundaries of model (Figure 6d). This regime occurs if the oceanic lithosphere is 50 Myr or older (Table 2 and Figure 10).

(b) Episodic short-lived circular subduction initiation

The plume breaks the lithosphere and a new plateau forms in the circular region created by plume penetration into the lithosphere. Descending of lithosphere into mantle starts as a result of negative buoyancy force due to the oceanic lithosphere and plume materials that are replaced atop of the lithosphere as well as density contrast at the plateau margin (Figure 7a indicating the compositional and stress fields of Model M25 in Table 2). Subducted slab breaks off at shallow depth (Figure 7b). A new downgoing circular slab forms behind the broken slab (Figure 7c). However, similar to the first short-lived slab, this subducted lithosphere is broken-off soon after its formation (Figure 7d). Our model results show that interaction of a plume with a young lithosphere (with the age of younger than 50 Myr) could result in episodic short-lived circular subduction initiation (Table 2 and Figure 10).

3.4. Effect of Mantle Plume With a Tail

We set-up some models in which we assume that the rising plume may bring some hot mantle materials with itself toward the surface. We simulate this by considering 200 K higher temperature at the lower model boundary. Figure 8 shows the compositional and stress fields of models M19 (which has a lithosphere of 20 Myr age with a crustal thickness of 8 km and present-day mantle temperature) and M78 that is similar to model M19 2 except that here a higher temperature below the mantle plume is considered. As the plume rises towards the surface hotter mantle rocks ascend below the plume. Subduction is formed faster in this model compared to model M19, which is a direct consequence of interaction of a more buoyant plume with the lithosphere which causes higher magmatic weakening. Due to continuous heating from the below, more mantle rucks are molten in this model compared to model M19. Outcomes of experiments with different lithospheric age, extension rate and thickness of the crust (Table 2, Models M60-M107) show that continuous rising of hot mantel materials towards

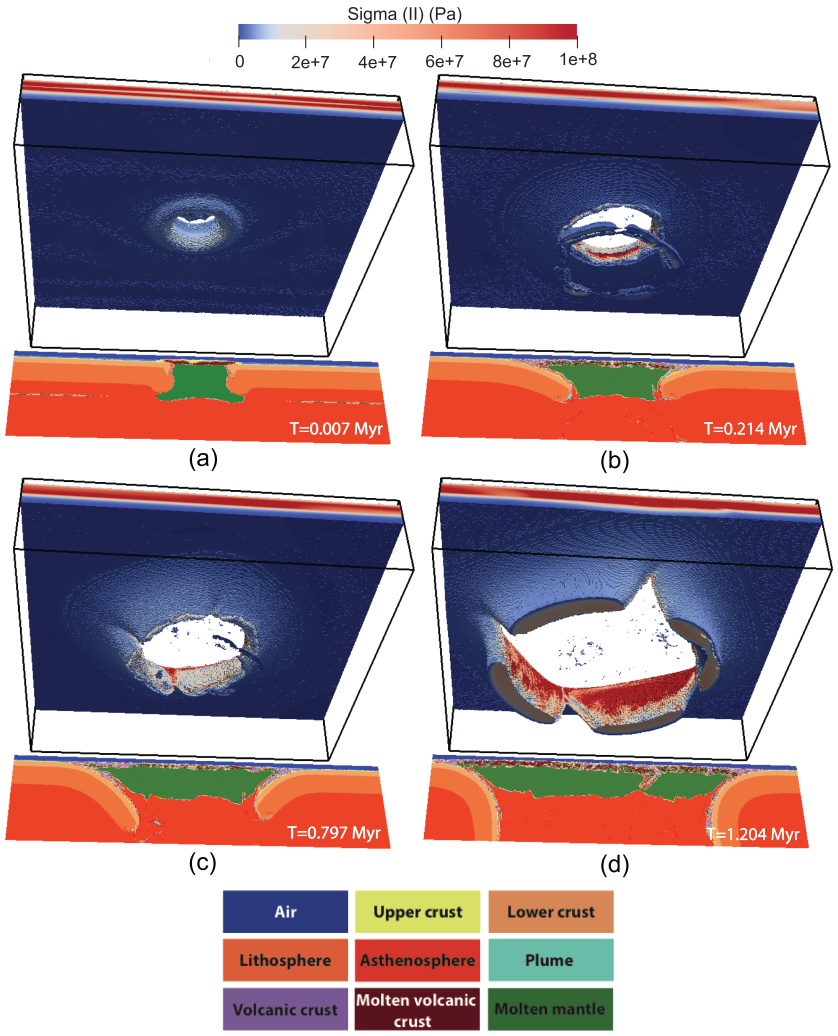

Figure 6. An example of models to investigate effect of mantle temperature (model M29 in Table 2) showing formation of multi-slab subduction initiation. For explanation of panel meanings, see Figure 2 caption.

the surface facilitates subduction initiation, especially when a mantle plume interacts with a lithosphere containing a thick plateau.

4. Discussion

4.1. General Models of Modern Earth

Results of our experiments for the present-day Earth show that plume-lithosphere interaction could result in three lithospheric deformation regimes that are formation of plateau without subduction initiation, single-slab subduction initiation and multi-slab subduction initiation. These lithospheric responses are governed by changes in several model parameters such as age of oceanic lithosphere, thickness of the crust, and extension rate. We acknowledge that several other parameters like plume buoyancy, which depends on the plume temperature, volume and chemical density likely affect the response of the lithosphere to the plume as well (Baes et al., 2016; Gerya et al., 2015; Ueda et al., 2008). We discuss some of these effects below but leave their detailed investigation for future studies.

To initiate subduction induced by plume-lithosphere interaction the first step is to break the lithosphere. Breaking of the lithosphere depends on several parameters such as plume volume, plume buoyancy and lithospheric thickness (Baes et al., 2016). In this study, a plume can break the lithosphere in all

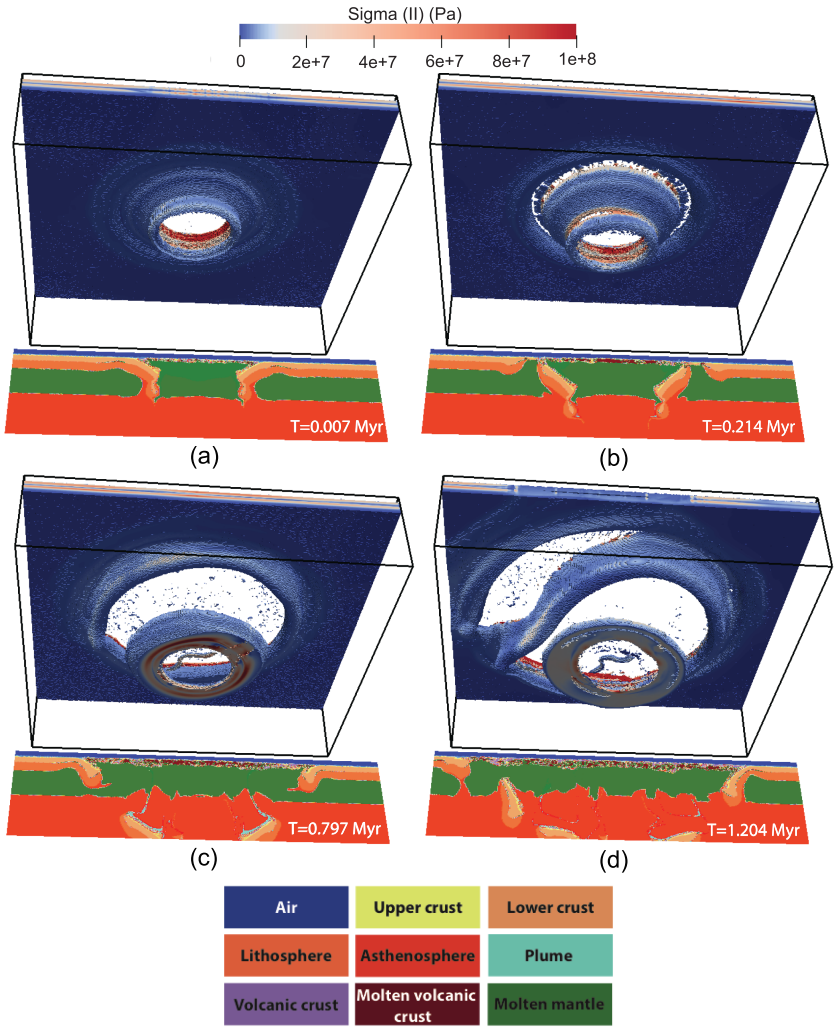

Figure 7. An example of models to investigate effect of mantle temperature (model M25 in Table 2) indicating formation of episodic short-lived circular subdution zone. For explanation of panel meanings, see Figure 2 caption.

experiments, indicating that the plume buoyancy is sufficient enough to overcome the lithospheric strength. Following breaking of the lithosphere, initiation of subduction depends on the subductability of the lithosphere, which is related to the strength and buoyancy of the lithosphere. Our experiments show that lowering the strength of the lithosphere by for instance imposing extension or interaction of lithosphere with a plume with a tail (which is more buoyant compared to a plume without a tail) can facilitate subduction initiation (see Figure 9, which summarizes the outcomes of our numerical study in terms of six regime diagrams). Negative buoyancy of the lithosphere, which acts as a driving force in subduction initiation, increases with decreasing of the crustal thickness and increasing of the lithospheric age. Interaction of a plume with a lithosphere with crustal thickness of 8 km, typical for the modern oceanic crust, may result in formation of multi-slab subduction if the oceanic lithosphere is young (age < 30 Myr for models with a plume with no tail and age < 40 Myr for models with a plume with a tail), but older than 10 Myr (Baes et al., 2016). When a mantle plume arrives beneath an older lithosphere with crustal thickness of 8 km, it may lead to formation of single-slab subduction. Plume-lithosphere interaction may lead to formation of plateau without subduction initiation if the lithosphere is older than 50 (Figures 9a and 9d). This indicates that although the aging of the lithosphere increases the negative buoyancy of the plate, its strength growth acts as a resistive force in subduction initiation process. We note that plume-induced subduction initiation of lithospheres older than 50 Myr maybe possible if a more buoyant plume interacts with the lithosphere (Baes et al., 2016; Gerya et al., 2015). Thicker oceanic crust hampers

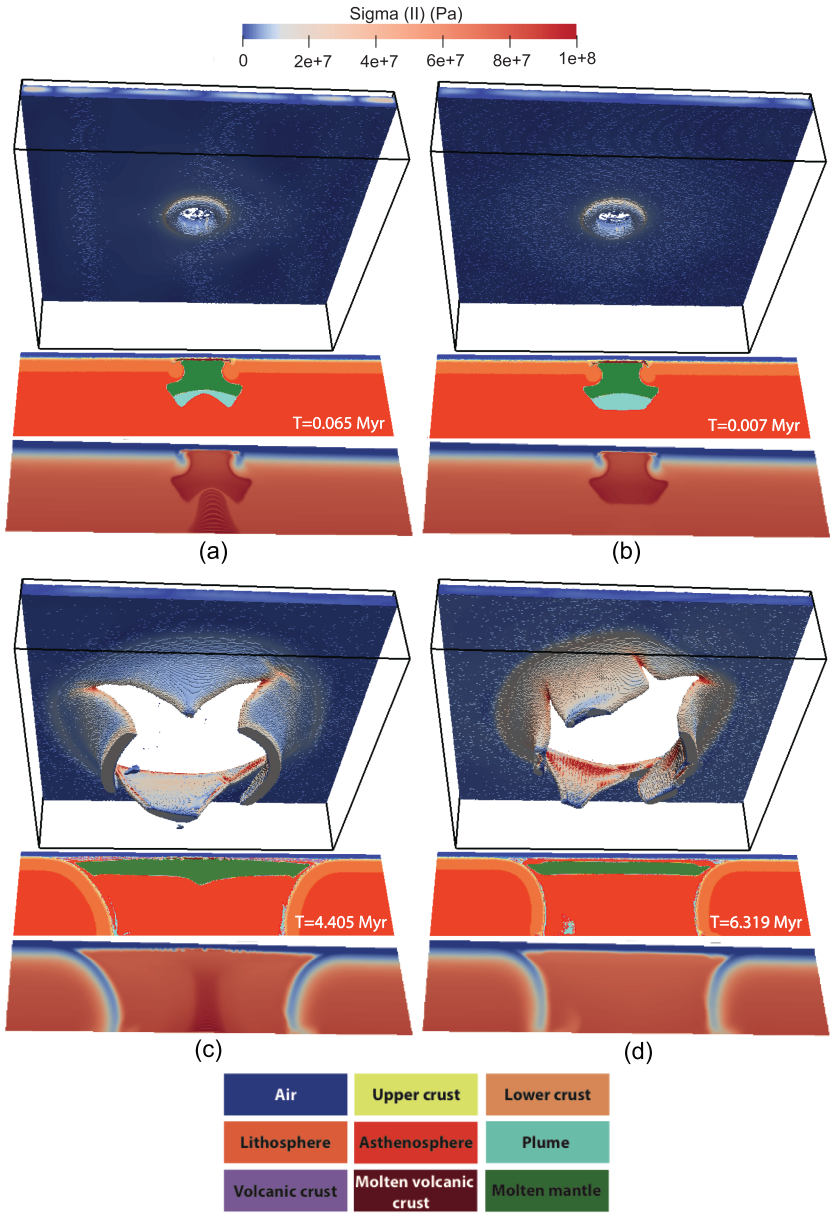

Figure 8. Effect of uprising of hot mantle materials below the plume. Panels (a) and (c), and (b) and (d) show the results of initial and final stages of models M78 and M19, respectively. For explanation of panel meanings, see Figure 2 caption.

subduction initiation due to its positive buoyancy, which increases resistance to subduction (Figures 9a and 9d). In models with a plume with no tail, subduction of plateau induced by plume-lithosphere interaction is rarely possible (Figure 9a). It occurs only if the crustal thickness and lithospheric age are 12 km and 40 Myr, respectively. In models with a plume with a tail, results of models with oceanic crustal thicknesses of more than 12 km show that subduction initiation induced by plume-lithosphere interaction occurs only if the age of oceanic lithosphere is 40 Myr. These results indicate the scarcity of formation of a new subduction zone induced by interaction of a mantle plume with a lithosphere containing a thick plateau.

Imposing extension can increase the subductability of oceanic lithosphere (Figures 9b-c9 and 9e-f9). Lithosphere with typical crustal thickness of 8 km under low extension rate show almost similar deformation regimes as those without extension, indicating the possibility of subduction of young oceanic

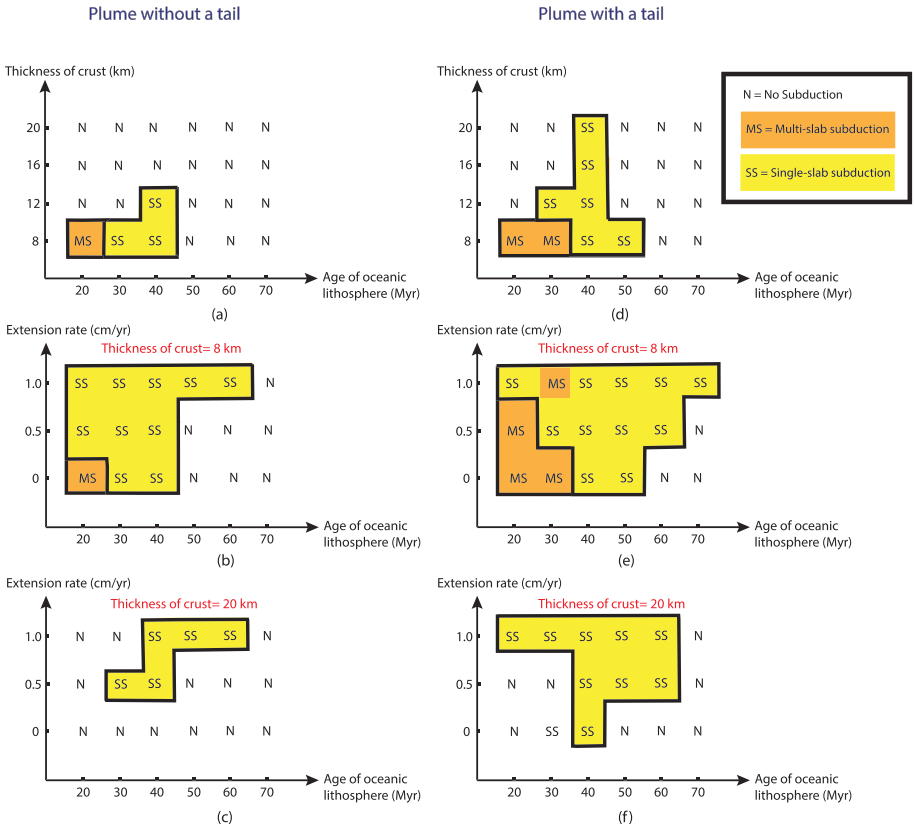

Figure 9. Summary of model results for present-day Earth. Effect of (a and d) thickness of the crust, (b and e) extension rate in models with 8 km crust, and (c and f) extension rate in models with 20 km crust. Panels (a)–(c) and (d)–(f) illustrate the results of models with a plume without and with a tail, respectively.

lithospheres (Figures 9b and 9e). However, higher extensional rate of 1 cm/yr enables formation of single-slab subduction also for the older lithospheres (Figures 9b and 9e). This is because fast extension reduces lithospheric strength. The same is true for the lithosphere with 20 km thick crust. In this case extension rate of 0.5–1 cm/yr enables subduction of moderately aged oceanic lithospheres (age = 30–60 Myr, Figure 9c).

The formation of single-slab or multi-slab subduction depends on the strength of the lithosphere. In models leading to development of multi-slab subduction, the strength of the slab is low due to its young lithosphere. As a result, ring confinement can be overcome by tearing of the low-strength slab at shallow depth (Figure S2 in supporting information data). However, in models resulting in formation of single-slab subduction, the failure of the lithosphere cannot occur at depth due to the high strength of the slab and depth dependency of the yield stress (equation (4) in section 2.). Therefore, in these models the ring confinement is overcome by breaking of the lithosphere (strain localization) at shallow depth from one side of the circular slab (Figure S3 in the supporting information data).

Comparing the results of models with a plume with and without a tail shows that subduction of a lithosphere containing a thick plateau becomes easier when a plume with a tail interacts with the lithosphere (Figure 9). The other effect of rising of a plume with a tail towards the surface is on the time of subduction initiation (Figure 8). Subduction is formed faster as a result of increasing of plume buoyancy, which leads to higher magmatic weakening. Multi-slab subduction, which requires a young and weak lithosphere, occurs more often in models simulating a plume with a tail.

In this study we simulate a plume head with a sphere of 200 km diameter. We note that comparison of model results with observations in the nature with the same plume radius depends on several parameters such as size of plume tail, amount of cold materials entrained into the plume head and plume composition.

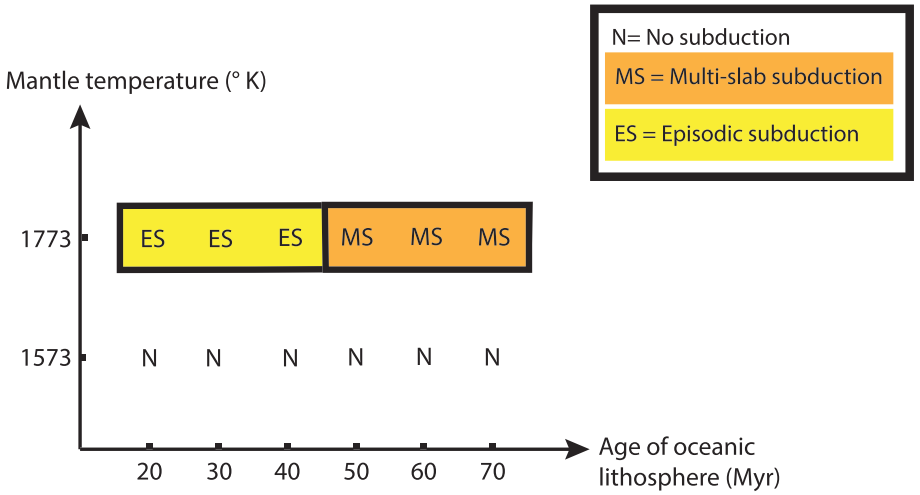

Figure 10. Summary of model results. Effect of mantle temperature in models with 20 km crust.

4.2. Application for the Early Earth

In Archean times the earth was 100–300 K hotter (Herzberg et al., 2010) and the crust was thicker than those in present day. We investigate the interaction of plume with Archean lithosphere assuming thickness of the oceanic crust of 20–30 km and higher mantle temperature of 1753 K. Figure 10 illustrates the results of models with average present-day mantle temperature (1573 K) along with outcomes of experiments with 200 K higher mantle temperature. The thickness of crust in all models is 20 km and the age of oceanic lithosphere is varying from 20–70 Myr.

Modeling results show that in contrast to present day where subduction initiation induced by interaction of a plume with a lithosphere containing a thick plateau is unlikely, plume-induced subduction initiation in the hot early Earth with thick crust was quite possible. Interaction of a plume with lithosphere in Archean times could result in either episodic and short-lived (young lithosphere) or multi-slab retreating (old lithosphere) subduction initiation, but not single-slab subduction zones, which should be common on modern Earth. These results are in good agreements with those in Gerya et al., 2015.

Fig 6 shows that initiation of multi-slab retreating subduction zones in hot early Earth was very efficient way to melt mantle and to produce new crust. We note that to allow initiation of multi-slab retreating subduction, early Earth lithosphere should have been older than 40–50 Myr. It means that just 40–50 Myr after the previous resurfacing the early Earth lithosphere was ready for the new extensive recycling and extensive formation of the new crust, triggered by arrival of large and hot enough mantle plume. This result confirms the recent suggestion that plume-induced retreating subduction zones was a plausible tectonic regime in Archean (Sobolev & Brown, 2019) when the rate of production of the crust was much higher than that on modern Earth (Dhuime et al., 2012).

4.3. Application for Caribbean

Whattam and Stern (2014) suggested plume-induced subduction initiation in the southern margin of the Caribbean and NW South America. They indicated that initiation of subduction was due to the presence of an old plateau (it was formed by plume-lithosphere interaction at 140–110 Ma), which created a pre-existing compositional and density contrast between the plateau and surrounding normal oceanic lithosphere. They also noted that the reason for single-slab subduction initiation (instead of multi-slab subduction) was the presence of subduction beneath the NE margin, which was formed some tens of million years before subduction initiation in western Caribbean. In this study we showed that formation of single-slab subduction depends on several parameters such as age of oceanic lithosphere, thickness of the crust and rate of extension (Figure 9). In contrary to Whattam and Stern (2014) we find that presence of plateau hinders plume-induced subduction initiation. However, our model results show that interaction of a plume with thick plateau can result in subduction initiation if the lithosphere is under extension.

Previous studies show that the oceanic lithosphere at the time of plume-lithosphere interaction in Caribbean (at 100 Ma) was older than 40 Myr (Gerya et al., 2015, and references therein). According to our model results in order to initiate single-slab subduction in Caribbean region plume might arrived either beneath a plateau, which was under extension, or beneath a lithosphere with crustal thickness of 8 km (see Figure 9). We point out that assumption of lithospheric extension some 100 Ma in Caribbean is plausible because the plume-lithosphere interaction in Caribbean occurred in the extensional back-arc region of the west dipping Puerto Rico/Lesser Antilles subduction zone (Whattam & Stern, 2014).

We note that it is not clear whether plume-lithosphere interaction in the Caribbean occurred within the pre-existing plateau or away from it. Here we assumed that the plume interacted with the lithosphere within the thick plateau. Further study is needed to investigate the effect of non-uniform crustal thickness and the location of plume head. We also studied the effect of a pre-existing subduction zone in the Caribbean region implicitly by considering the effect of extension in its back-arc. Exploring the effect of pre-existing subduction on plume-lithosphere interaction in more details requires models with different model setup and larger dimensions, which is worth to be investigated in future studies.

5. Conclusions

Using 3-D thermo-mechanical models we have shown that the response of the lithosphere to arrival of a mantle plume beneath it depends on several parameters such as age of oceanic lithosphere, thickness of the crust, extension rate, and mantle temperature. The numerical experiments revealed that plume-lithosphere interaction in present day Earth can result in three different deformation regimes: (a) multi-slab subduction initiation, (b) single-slab subduction initiation, and (c) plateau formation without subduction initiation. On early Earth (in Archean times) plume-lithosphere interaction could result in formation of either multi-slab subduction zones, very efficient in production of new crust, or episodic short-lived circular subduction. The former occurs if the lithosphere is older than 50 Myr and the latter refers to the interaction of a plume with a younger lithosphere. In contrary to the early Earth, in present-day Earth, multi-slab subduction zones can be initiated only if a plume hits a relatively young oceanic lithosphere (<40 Myr but older than 10 Myr). We found that extension eases subduction initiation caused by plume-lithosphere interaction. Plume-induced subduction initiation of old oceanic lithosphere with a plateau with thick crust is only possible if the lithosphere is subjected to extension. Interaction of lithosphere with a plume that features a plume tail also facilitates subduction initiation. We suggest that single-slab subduction in the eastern Caribbean was formed due to either plume-plateau interaction in an extensional regime or arrival of a mantle plume beneath a lithosphere with typical crustal thickness of 8 km.

Acknowledgments
This work has been funded by the German Science Foundation (DFG) (Project BR 5815/1-1). The computational resources were provided by the North German Supercomputing Alliance (HLRN). The data regarding experiments in this study have been provided in GFZ data services (https://webmail.gfz-potsdam.de/Redirect/5292A2DA/doi.org/10.5880/GFZ.2.5.2019.002).

References

Baes, M., Gerya, T. V., & Sobolev, S. V. (2016). 3-D thermo-mechanical modeling of plume-induced subduction initiation. *Earth and Planetary Science Letters*, *453*, 193–203.

Bercovici, D. (2003). The generation of plate tectonics from mantle convection. *Earth and Planetary Science Letters*, *205*, 107–121. https://doi.org/10.1016/S0012-821X(02)01009-9

Boschman, L. M., van der Wiel, E., Flores, K. E., Langereis, C. G., & van Hinsbergen, D. J. J. (2019). The Caribbean and Farallon plates connected: Constraints from stratigraphy and paleomagnetism of the Nicoya Peninsula, Costa Rica. *Journal of Geophysical Research - Solid Earth*, *124*, 6243–6266. https://doi.org/10.1029/2018JB016369

Burov, E., & Cloetingh, S. (2010). Plume-like upper mantle instabilities drive subduction initiation. *Geophysical Research Letters*, *37*, L03309. https://doi.org/10.1029/2009GL041535

Byerlee, J. (1978). Friction of rocks. *Pure and Applied Geophysics*, *116*, 615–626.

Cloetingh, S. A. P. L., Wortel, M. J. R., & Vlaar, N. J. (1982). Evolution of passive continental margins and initiation of subduction zones. *Nature*, *297*, 139–142.

Cloetingh, S. A. P. L., Wortel, M. J. R., & Vlaar, N. J. (1984). Passive margin evolution, initiation of subduction and the Wilson cycle. *Tectonophysics*, *109*, 147–163.

Cloetingh, S. A. P. L., Wortel, M. J. R., & Vlaar, N. J. (1989). On the initiation of subduction zone. *Pageoph*, *129*, 7–25.

Connolly, J. A. D., Schmidt, M. W., Solferino, G., & Bagdassarov, N. (2009). Permeability of asthenospheric mantle and melt extraction rates at mid-ocean ridges. *Nature*, *462*, 209–214.

Cowley, S., Mann, P., Coffin, M. F., & Shipley, T. H. (2004). Oligocene to Recent tectonic history of the Central Solomn intra-arc basin as determined from marine seismic reflection data and compilation of onland geology. *Tectonophysics*, *389*(3-4), 267–307. https://doi.org/10.1016/j.tecto.2004.01.008

Dhuime, B., Hawkesworth, C. J., Cawood, P. A., & Storey, C. D. (2012). A change in the geodynamics of continental growth 3 billion years ago. *Science*, *335*(6074), 1334–1336. https://doi.org/10.1126/science.1216066

Faccenna, C., Giardini, D., Davy, P., & Argentieri, A. (1999). Initiation of subduction at Atlantic-type margins: Insights from laboratory experiments. *Journal of Geophysical Research*, *104*(B2), 2749–2766. https://doi.org/10.1029/1998JB900072

Gerya, T. (2010). *Introduction to numerical geodynamic modelling*. Cambridge: Cambridge University Press.

Gerya, T. V. (2013). Three-dimensional thermomechanical modeling of oceanic spread-ing initiation and evolution. *Physics of the Earth and Planetary Interiors*, *214*, 35–52.
Gerya, T. V., & Meilick, F. I. (2011). Geodynamic regimes of subduction under an active margin: Effects of rheological weakening by fluids and melts. *Journal of Metamorphic Geology*, *29*, 7–31.
Gerya, T. V., Stern, R. J., Baes, M., Sobolev, S. V., & Whattam, S. A. (2015). Plume-induced subduction initiation triggered Plate Tectonics on Earth. *Nature*, *527*(7577), 221–225. https://doi.org/10.1038/nature15752
Gurnis, M., Hall, C., & Lavier, L. (2004). Evolving force balance during incipient subduction. *Geochemistry, Geophysics, Geosystems*, *5*, Q07001. https://doi.org/10.1029/2003GC000681
Hall, C. E., Gurnis, M., Sdrolias, M., Lavier, L. L., & Muller, R. D. (2003). Catastrophic initiation of subduction following forced convergence across fracture zones. *Earth and Planetary Science Letters*, *212*, 15–30.
Hathway, W. B. (1993). The Nadi Basin: Neogene strike-slip faulting and sedimentation in a fragmented arc, western Viti Levu, Fiji. *Journal of the Geological Society, London*, *150*, 563–581.
Herzberg, C., Condie, K., & Korenaga, J. (2010). Thermal history of the Earth and its petrological expression. *Earth and Planetary Science Letters*, *292*, 79–88.
Ito, K., & Kennedy, G. C. (1971). An experimental study of the basalt-garnet granulite-eclogite transition. In J. G. Heacock (Ed.), *The structure and physical properties of the Earth's crust*, *Geophys. Monograph Series*, (Vol. 14, pp. 303–314). WAshington, D. C: Am. Geophys. Union.
Kroenke, L. W. (1989). Interpretation of a multi-channel seismic reflection profile northeast of the Solomon Islands from the southern flank of the Ontong Java Plateau across the Malaita anticlinorium to the Solomon Islands arc. In J. G. Vedder, & T. R. Bruns (Eds.), *Geology and offshore Resources of Pacific Island Arcs-Solomon Islands and Bougainville, Papua New Guinea region*, *Earth Science Series*, (Vol. 12, pp. 145–148). Houston, Texas: Circum-Pacific Council for Energy and Mineral Resources.
Lebrun, J.-F., Lamarche, G., & Collot, J.-Y. (2003). Subduction initiation at a strike-slip plate boundary: The Cenozoic Pacific-Australian plate boundary, south of New Zealand. *Journal of Geophysical Research*, *108*(B9), 2453. https://doi.org/10.1029/2002JB002041
McKenzie, D. P. (1977). Initiation of trenches: A finite amplitude instability. In M. Talwani, & W. Pitman (Eds.), *Island Arcs, Deep Sea Trenches and Back-Arc basins*, *Maurice Ewing Series*, (Vol. 1, pp. 57–62). Washington, D. C: American Geophysical Union.
Mueller, S., & Phillips, R. J. (1991). On the initiation of subduction. *Journal of Geophysical Research*, *96*, 651–665.
Nikolaeva, K., Gerya, T. V., & Marque, F. O. (2010). Subduction initiation at passive margins: Numerical modeling. *Journal of Geophysical Research*, *115*, B03406. https://doi.org/10.1029/2009JB006549
Pearce, J. A., van der Laan, S. R., Arculus, R. J., Murton, B. J., Ishii, T., Peate, D. W., & Parkinson, I. J. (1992). Boninite and harzburgite from Leg 125 (Bonin-Mariana Forearc): A case study of magma genesis during the initial stages of subduction. In L. B. Stokking (Ed.), *Proc. Ocean Drill. Prog., Sci. Results* (Vol. 125, pp.623–659). College Station, TX: Ocean Drilling Program. https://doi.org/10.2973/odp.proc.sr.125.172.1992
Phinney, E. J., Mann, P., Coffin, M. F., & Shipley, T. H. (2004). Sequence stratigraphy, structural style, and age of deformation of the Malaita accretionary prism (Solomon arc -Ontong Java plateau convergent zone). *Tectonophysics*, *389*, 221–246.
Ranalli, G. (1995). *Rheology of the Earth*. Science and Business Media, London: Springer.
Regenauer-Lieb, K., Yuen, D. A., & Branlund, J. (2001). The initiation of subduction: Criticality by addition of water? *Science*, *19*, 578–580.
Sobolev, S. V., & Brown, M. (2019). Surface erosion events controlled the evolution of plate tectonics on Earth. *Nature*, *570*(7759), 52–57. https://doi.org/10.1038/s41586-019-1258-4
Stern, R. J. (2004). Subduction initiation: Spontaneous and induced. *Earth and Planetary Science Letters*, *226*, 275–292.
Stern, R. J., & Dumitru, T. A. (2019). Eocene initiation of the Cascadia subduction zone: A second example of plume-induced subduction initiation? *Geosphere*, *15*, 659–681.
Stern, R. J., & Gerya, T. (2018). Subduction initiation in nature and models: A review. *Tectonophysics*, *746*, 173–198.
Turcotte, D., & Schubert, G. (1982). *Geodynamics: Applications of continuum physics to geological problems*, (p. 450). New York: John Wiley.
Ueda, K., Gerya, T. V., & Sobolev, S. V. (2008). Subduction initiation by thermal–chemical plumes: Numerical studies. *Physics of the Earth and Planetary Interiors*, *171*(1), 296–312.
Uyeda, S., & Ben-Avraham, Z. (1972). Origin and development of the Philippine Sea. *Nature*, *240*, 176–178.
Wells, R. E. (1989). Origin of the oceanic basalt basement of the Solomon Islands arc and its relationship to the Ontong Java Plateau-insights from Cenozoic plate motion models. *Tectonophysics*, *165*, 219–235.
Whattam, S. A., & Stern, R. J. (2014). Late Cretaceous plume-induced subduction initiation along the southern margin of the Caribbean and NW South America: The first documented example with implications for the onset of plate tectonics. *Gondwana Research*, 27. https://doi.org/10.1016/j.gr.2014.07.011
Wilson, J. T. (1966). Did the Atlantic close and then re-open? *Nature*, *211*, 676–681.
Yan, C. Y., & Kroenke, L. W. (1993). A plate-tectonic reconstruction of the southwest Pacific, 100-0 Ma. *Ocean Drilling Program Proceedings, Scientific Results*, *130*, 697–710.